Published in final edited form as:

ACS Biomater Sci Eng. 2020 January 13; 6(1): 505–516. doi:10.1021/acsbiomaterials.9b00861.

Electrospun Polyurethane–Gelatin Composite: A New Tissue-Engineered Scaffold for Application in Skin Regeneration and Repair of Complex Wounds

Mohammadali Sheikholeslam[†,‡,§], **Meghan E. E. Wright**[‖], **Nan Cheng**[†,‡], **Hwan Hee Oh**[†,‡], **Yanran Wang**[†,‡], **Andrea K. Datu**[†], **J. Paul Santerre**[*,‖,⊥], **Saeid Amini-Nik**[*,†,‡,#], **Marc G. Jeschke**[*,†,‡,¶]

[†]Ross Tilley Burn Centre, Sunnybrook Research Institute, Sunnybrook Health Sciences Centre, University of Toronto, 2075 Bayview Avenue, Toronto, Ontario M4N 3M5, Canada

[‡]Department of Surgery, Immunology, Division Plastic Surgery, University of Toronto, Toronto, Ontario M5S 3K1, Canada

[‖]Institute of Biomaterials & Biomedical Engineering, Translational Biology and Engineering Program, Ted Rogers Centre for Heart Research, University of Toronto, Toronto, Ontario M5S 3K1, Canada

[⊥]Faculty of Dentistry, University of Toronto, Toronto, Ontario M5S 3K1, Canada

[#]Department of Laboratory Medicine and Pathobiology, University of Toronto, Toronto, Ontario M5S 3K1, Canada

[¶]Institute of Medical Science, University of Toronto, Toronto, Ontario M5S 3K1, Canada

[§]Department of Biomaterials, Tissue Engineering and Nanotechnology, School of Advanced Technologies in Medicine, Isfahan University of Medical Sciences, Isfahan, Isfahan 81746-73461, Iran

Abstract

Wound healing is vital for patients with complex wounds including burns. While the gold standard of skin transplantation ensures a surgical treatment to heal wounds, it has its limitations, for example, insufficient donor sites for patients with large burn wounds and creation of wounds and pain when harvesting the donor skin. Therefore, tissue-engineered skin is of paramount importance. The aim of this study is to investigate and characterize an elastomeric acellular scaffold that would demonstrate the ability to promote skin regeneration. A hybrid gelatin-based electrospun scaffold is fabricated via the use of biodegradable polycarbonate polyurethane (PU). It is hypothesized that the addition of PU would enable a tailored degradation rate and an enhanced mechanical strength of electrospun gelatin. Introducing 20% PU to gelatin scaffolds (Gel80–PU20) results in a significant increase in the degradation resistance, yield strength, and elongation of these scaffolds without altering the cell viability. In vivo studies using a

[*]**Corresponding Authors:** paul.santerre@dentistry.utoronto.ca (J.P.S.); saeid.amininik@utoronto.ca (S.A.-N.); marc.jeschke@sunnybrook.ca (M.G.J.).

The authors declare no competing financial interest.

mouse excisional wound biopsy grafted with the scaffolds reveals that the Gel80–PU20 scaffold enables greater cell infiltration than clinically established matrices, for example, Integra (dermal regeneration matrix, DRM), a benchmark scaffold. Immunostaining shows fewer macrophages and myofibroblastic cells on the Gel80–PU20 scaffold when compared with the DRM. The findings show that electrospun Gel80–PU20 scaffolds hold potential for generating tissue substitutes and overcoming some limitations of conventional wound care matrices.

Graphical Abstract

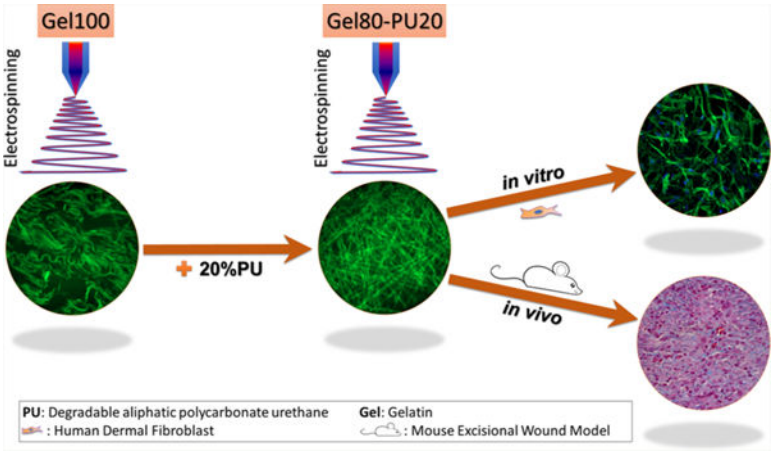

Keywords

gelatin–polycarbonate urethane; biodegradable; electrospinning; tissue engineering; skin regeneration

1. INTRODUCTION

Patient survival with significant burn injuries and associated skin loss is directly linked with wound healing and skin regeneration.[1–5] Although in superficial burn wounds, the skin can heal, in deeper injuries, when the dermis is compromised, it cannot heal and self-regenerate to its primary condition.[6,7] In these cases, the burned skin needs to be excised, and the wound needs to be covered with autologous skin grafts. Split-thickness skin grafts are normally thinner than native skin and are associated with creating more wounds (donor site), pain, and scarring as well as have poor cosmetic outcomes.[3,7,8] Therefore, split-thickness skin grafting has major limitations. An additional challenge, particularly in patients with burns over 30–40% of their total body surface, is the lack of sufficient donor sites. In these cases, autografting has to be conducted in several stages; it heavily depends on the donor sites' ability to heal back to a healthy state, which can take long times, or sometimes, the donor site converts and becomes a wound itself. In these cases, the patient's life is at risk as the burn wounds cannot be closed; therefore, the development of tissue-engineered skin substitutes is imperative to improve burn patient outcomes.[9]

When designing a skin substitute, the anatomy and physiology of the skin have to be accounted for. Skin is comprised of two distinct layers that are physically separated by

the basement membrane: a dermal layer made of a fibrous network of extracellular matrix (ECM) proteins, mainly collagen and elastin, which provides physical strength and absorbs stress, and an epidermal layer which acts as the barrier to exogenous substances and infections and prevents dehydration of the body.[10,11] The main cell type in the dermis is fibroblasts, whereas keratinocytes make up the majority of cells that form the epidermis.[12,13]

To date, clinically available dermal skin substitutes or dermal replacement matrices consist mainly of biological materials. Some of these are purely made of biological material (e.g., AlloDerm, Glyaderm, and Permacol), whereas others include synthetic barrier polymers as well, such as Integra, Matriderm, Hyalomatrix, Dermagraft, and TransCyte.[7,10,11] All of these materials have their own limitations, which include the need for a second surgery, risk of remnant cells from allogenic sources, transmitting infectious diseases, eliciting immune response, associated scarring, and in most cases, high cost.[7] Integra (DRM; dermal regeneration matrix) is the most commonly used scaffold for burn patients.[7] It has a bilayer structure including spongelike bovine collagen I matrix containing chondroitin sulfate, which provides the dermal layer, and a synthetic nondegradable silicon layer as a temporary cover (epidermal layer) and a barrier for wound infection.[14] As aforementioned, dermal replacement matrices have several drawbacks including their high cost and risk of infection and subsequent failure.[7,14] Hence, there is still a clinical need for a reliable but yet economically viable skin substitute that can lead to accelerated and scarless skin regeneration while developing skin appendages.[15]

Among the different fabrication methods that have been employed for the engineering of three-dimensional (3D) scaffolds,[14,16–18] electrospinning has been shown to be versatile because of its adaptability to large-scale production, simplicity, and availability, all factors which contribute to cost-effectiveness.[19–21] Using electrospinning, one can generate fibrous scaffolds with controlled thickness, highly interconnected pores, and high surface area.[20–22] Considering the fibrous structure of the dermis, this technique is an excellent option for generating dermal scaffolds.[23]

Gelatin is a denatured form of collagen, the main component of the dermis. It has great potential for electrospinning and is much less costly than collagen and elastin and other dermal components.[24–26] Moreover, it is considered to be broadly biocompatible and shows cell-adherence.[27–29] However, like other natural biopolymers, gelatin suffers from poor mechanical strength which limits its handling. Further, it has very fast degradation rates. It must be emphasized that mechanical properties are important, because poor elasticity and mechanical strength in a skin substitute contributes to scarring and wound contracture.[30,31] We hypothesized that by blending an elastomeric polyurethane (PU), that could undergo controlled degradation, with gelatin to contribute to cohesion between the biopolymer and the synthetic polymer, we would improve the mechanical strength and elasticity of tissue-engineering scaffolds and hence yield good regenerative outcomes.

PUs are widely used biomaterials because of their excellent elasticity and tailored biocompatibility. Polycarbonate-urethanes are biodegradable elastomeric biomaterials which primarily generate diols and CO_2 as their final degradation products.[32–34] Further, their urethane groups provide hydrogen-bonding domains for interaction with proteins such as

gelatin and have the potential to provide good cohesion between the polymers. These polymers can also be electrospun into fibrous scaffolds, with excellent cell compatibility, controlled degradation, and nontoxic degradation products.[35,36] As such, a polycarbonate PU previously used for tissue-engineering applications of spinal disc tissue engineering[35,36] was chosen as a copolymer for electrospinning with gelatin skin tissue-engineering scaffolds. The goal of this work was to introduce PUs into the gelatin in order to delay the degradation rate of gelatin scaffolds and to compensate for an inherent lack of mechanical strength while still retaining good cell compatibility. There are currently only a few studies published on the use of gelatin–PU scaffolds in the literature,[37–42] however, neither study has reported on skin tissue applications or the use of degradable PUs generating non-acid byproducts.[43–47] Note that membranes with a high content of PU are typically not desired as these materials often take too long to fully degrade[36] for skin regeneration applications, where it is desired to have regeneration of tissue within 30 days.[7] Hence, there is an opportunity to investigate membranes which contain PU at low concentrations for skin regeneration scaffolds.

In the current study, a biodegradable, nontoxic, and elastic degradable polycarbonate-based PU was incorporated via blend electrospinning with gelatin at an 80/20 mass ratio of gelatin to PU (herein referred to as Gel80–PU20), and the gelatin–PU blend scaffolds were compared to 100% gelatin scaffolds (Gel100), given that it was desired to improve upon this latter material. It was desired to compare the results to a commercially available skin substitute material, referred to as DRM (Table 1). One of the main goals of this study was to improve the performance and suitability of gelatin, which is a very weak material relative to collagen, while yielding minimal changes to its favorable structure features.

2. RESULTS

2.1. Scaffold Morphology.

The physical morphology of the as-spun scaffolds was examined by scanning electron microscopy (SEM) (Figure 1a,b). The electrospinning parameters were adjusted with respect to solution viscosity (changing concentration to achieve reproducibility) and charge in order to yield electrospun Gel80–PU20 and Gel100 scaffolds that had a similar average fiber size (~2 μm) (Figure 1c). There were no significant differences in the typical interfiber distance for Gel100 and Gel80–PU20 (12.9 ± 6.6 vs 14.5 ± 6.1 μm, respectively) (Figure 1d).

2.2. Attenuated Total Reflectance Fourier Transform Infrared.

Attenuated total reflectance Fourier-transform infrared (ATR–FTIR) spectroscopy was performed on the as-spun samples. Gelatin showed typical protein-associated peaks in the 1530 and 1630 cm^{-1} regions, related to amide II and amide I bonds, respectively (Figure S2). In order to identify the peaks specifically related to the PU, an electrospun 100% PU spectrum was generated. It exhibited a large peak in the 1200–1280 cm^{-1} region, which was assigned to the carbonate ether stretching, whereas peaks in the 1650–1800 cm^{-1} region were assigned to its carbonyl groups. The peak in the 3300–3400 cm^{-1} region was assigned to its amine groups (Figure S2). Characteristic peaks indicative of gelatin and PU were denoted in the spectrum of the Gel80–PU20 membrane. Although dominant gelatin peaks

were present for Gel80–PU20 up to 7 days, the latter showed a significant change in 14 days, whereas the PU peaks were relatively intact. Also, it was observed that Gel100 had a spectrum very similar to that of DRM, and the cross-linking of the Gel80–PU20 scaffold did not alter the presence of these peaks (Figure S2).

2.3. Scaffold Swelling.

The swelling index of the gelatin–PU composite is compared to gelatin in Figure 1e. This parameter is indicative of the hydrating capacity of the scaffold, which is an important factor in wound healing in terms of absorbing wound exudates and also preventing the wound from drying. While the literature is not conclusive on how much moisture capacity is needed, it is acknowledged that the scaffold hydration must be retained.[9] Values on the vertical axis show that the swelling index [the ratio of absorbed Dulbecco's modified Eagle medium (DMEM) media to the initial mass of the scaffold] decreases slightly from 15.8 ± 0.5 for G100 to 10.0 ± 0.7 for Gel80–PU20. This drop is reflective of the exchange of 20% of gelatin with PU, which is comparatively more hydrophobic[48] with a less hydration capacity than gelatin because of its chemistry. Note that the electrospun fibers both initially show significantly less moisture uptake in comparison to traditional collagen-based DRM materials (e.g., Integra DRM showed a swelling index of 49.5 ± 4.6). This difference is believed to be primarily related to the large pore size and/or chemical composition (e.g., presence of chondroitin sulfate, which is negatively charged and as such attracts water molecules) associated with DRM.[49] The larger pore structure of DRM was confirmed by SEM in Figure S1. It should be noted that the pore structure is a temporal effect which will change as the scaffold undergoes hydrolysis (Figure S3), as discussed in Section 2.5, and hence, one would anticipate that moisture uptake will further improve for the scaffolds with time.

2.4. Mechanical Properties.

Microtensile testing was used to determine the mechanical properties of the hydrated scaffold, and the data for the test materials were compared to DRM (Figure 1f–h). DRM is a relatively stiffer material and yielded the highest elastic modulus (388 ± 45 kPa). Stiffness is a parameter which affects the contractile state of fibroblasts.[50] Gel100 showed the lowest elastic modulus (130 ± 10 kPa), while the introduction of 20% PU by weight into Gel80–PU20 increased the elastic modulus to 260 ± 11 kPa. The ultimate tensile strength (UTS) values for DRM and Gel80–PU20 were very comparable to each other (79 ± 7 and 94 ± 12 kPa), whereas that of Gel100 was 25 ± 1 kPa. Gel80–PU20 showed the greatest elongation at break (60.7 ± 4.8), whereas this parameter was similar for both DRM (34.6 ± 4.1) and Gel100 (34.7 ± 7.7). Hence, the introduction of a small amount of degradable PU into Gel80–PU20 significantly enhanced the mechanical properties of cross-linked gelatin.

2.5. In Vitro Degradation.

The in vitro enzymatic degradation study of Gel80–PU20 was compared to Gel100 and DRM, using a collagenase solution in phosphate-buffered saline (PBS) at 37 °C and incubated for just over 14 days. The results are reported in Figure 1i. Gel100 showed the highest degradation rate and was completely dissolved within 3 h. This is an inherent challenge with gelatin and one that was sought to be corrected with the introduction of PU.

The presence of 20% PU in the gelatin structure significantly stabilized the scaffold and enhanced its degradation resistance to be more closely aligned with that of DRM up to 7 days. The results show that the weight loss increases for both Gel80–PU20 and DRM over time but that DRM was more resistant to the elevated in vitro levels of collagenase used in the current study. In agreement with the mass loss measurements, the FTIR results after the degradation test (Figure 1j) show that the characteristic peak of gelatin had disappeared by day 14, whereas the peak that corresponded to PU was still clearly visible. Images of the scaffolds as they degraded are shown in Figure S3, where both DRM and Gel80–PU20 retain physical aspects of their integrity up to 7 days, G80–PU20 shows the greatest change at 14 days, and Gel100 is gone well before 7 days.

Further evidence of the inherent physical stability for the acellular scaffolds was shown when the samples were incubated in DMEM cell culture media at 37 °C for 7 days and imaged by confocal microscopy. Because all scaffolds autofluoresced at very high intensity and prolonged exposure during imaging, it was possible to apply this condition to see the rapid loss of fiber structure for the Gel100 fibers in comparison to the Gel80–PU20 fibers (Figure 1k).

2.6. Cell–Scaffold Interaction.

An ideal scaffold should allow cells to infiltrate and proliferate in order to cellularize and generate tissue within the full thickness of the scaffold. As such, confocal microscopy was used to characterize the cell–scaffold interaction. Human dermal fibroblasts (HDFs) cultured for 7 days in the scaffolds were fixed and stained for F-actin with ActinGreen (green) and for nuclei with 4′,6-diamidino-2-phenylindole (DAPI) (blue) (Figure 2a). The cytoskeleton of the cells was imaged by the green stain (Figure 2a). Cells were highly aligned within the Gel100 scaffold, whereas they were randomly oriented on Gel80–PU20 and DRM. This is confirmed by cell orientation measurements using Sedeen Viewer software and is shown in Figure S4. In contrast with DRM, the cells are spindlelike on the electrospun scaffolds.

Figure 2b displays a confocal *z*-stack for all three scaffolds and confirmed cell infiltration. Although there are a few cells which have penetrated more deeply into DRM (likely due to very large pores), the majority of cell penetration after 7 days was similar for all three materials, approximately 75 μm into the scaffold (Figures S4d). This suggests that as the cells and related enzymes resorb the gelatin, the path is cleared for cells and hydration fluids.

2.7. Live/Dead Assay.

Live/Dead staining was performed after 7 days of culturing HDFs in the scaffolds (Figure S5). Cell viability on all of the scaffolds was greater than 90%, and there were no statistically significant differences between each scaffold type (Figure 2c). When compared to the Gel100 and Gel80–PU20 scaffolds, the cell surface coverage on the scaffold for DRM was less dense. This may be attributed in part to the differences in material presented to the cells, with the high surface area of the fibers providing a substrate resembling typical ECM fiber structures[9] for the cells to attach to. This is in contrast to the walled cavity of the large pore DRM structure.

2.8. In Vivo Experiments.

Because of the poor physical, biological, and biochemical properties of the Gel100 scaffold revealed during the in vitro studies (i.e., fast degradation rate, insufficient mechanical strength, and elevated myofibroblastic character) and consideration for animal ethics, we elected to only pursue the in vivo characterization of the scaffolds with Gel80–PU20 to compare it to that of the established DRM. Using a recently reported surgical mouse model for skin regeneration,[51] we grafted acellular scaffolds into two 8 mm skin punch biopsies in each mice. The acellular system is the established protocol traditionally used for materials such as the commercial DRM selected for the current study.[51] Animals were sacrificed after 20 days, and the tissues were collected and sectioned for further analysis. Masson's trichrome staining that was performed on wounds covered with Gel80–PU20 (Figure 3a) revealed that the structure of the scaffolds was well integrated right into the wound bed [note the electrospun fibers stained gray (black arrows)]. As a control reference of the scaffold alone, trichrome staining of the Gel80–PU20 scaffold after incubation in cell culture media is shown in Figure S6 for reference. Further, a SEM image of the cross-section of the electrospun Gel80–PU20 membrane obtained after snap-freezing and breaking is provided in Figure S7 for reference.

In Figure 3a, the fibrous structure was more intact in the upper area of the scaffold than lower in the bed. Hematoxylin and eosin (H&E) staining was also performed and showed similar results as seen in trichrome staining (Figure S8). Both scaffolds showed well-distributed cell infiltration into the scaffold (Figure 3a,b). Both of the scaffolds promoted collagen deposition and vascularization as indicated with arrow heads and white circles (Figure 3a). A CD31 marker was used in immunohistochemistry (IHC) to stain endothelial cells. Blood vessel population and area were measured, and no significant difference was observed in the two wounds grafted by Gel80–PU20 and DRM in terms of blood vessel population. However, the blood vessel total area was greater for DRM as compared with that of the electrospun scaffold (Figure 3c,d). The electrospun scaffold showed a greater cell density than DRM (Figure 3e). Residual scaffold in vivo was measured on H&E stained sections, and the data was reported as %degradation (as measured by area) (Figure 3f). The data showed significantly more degradation in the electrospun scaffold as compared to the DRM. Figure S9 shows two representative H&E images and the calculated residual scaffold area.

F4/80 staining for immunofluorescence (IF) imaging showed that macrophages (stained in red) are mainly enriched in the wound bed, especially in the case of Gel80–PU20 (Figure S10). Unlike the DRM scaffold, significantly fewer macrophages are seen within the Gel80–PU20 scaffold (Figure 4a). This was also confirmed by IHC staining provided in Figure S11. Furthermore, sections were stained for MHC class II as a marker of type 1 macrophages (M1: pro-inflammatory) and CD206 as a marker of type 2 macrophages (M2: anti-inflammatory). The results showed that both M1 and M2 were present in the scaffolds (Figure 4b). Also, similar to F4/80 staining data, more macrophages (of either type) were found on the DRM scaffold.

Sections were immune-stained for α-smooth muscle actin (α-SMA) as a marker of myofibroblasts and showed significantly fewer α-SMA fluorescent cells (stained in red)

in the wound covered by the Gel80–PU20 scaffold when compared with that of the DRM (Figure 4c). Although the presence of the dome on the wound prevents wound contraction and is an ideal model for evaluating dermis reconstitution, it does hamper wound closure and epithelialization, and therefore, the latter needs to be accommodated for in the interpretation of the data. Hence, in order to confirm wound closure in the absence of a dome on the wounds, scaffolds grafted on the wounds without using domes and fixed in place were also reported on. The results show that the wound closes after 14 days for both the scaffolds (Figure S13).

3. DISCUSSION

Designing scaffolds that include the essential components of biodegradability and mechanical properties, while promoting tissue regeneration and viable cell function, is a major challenge in the field of skin repair. The results of the present study have demonstrated that the introduction of a degradable and cell compatible PU at an 80/20 mass ratio of gelatin to PU does not induce a change in the dimensions of the fiber or the construct's typical interfiber distance, relative to that of an electrospun gelatin scaffold. Further, the introduction of the PU enabled effective cell integration and ECM production across the membranes. Given the similarity in the typical interfiber distance, we can conclude that any enhanced outcome for seeded cells on Gel80–PU20 scaffolds versus Gel100 was related primarily to changes in the chemistry of the composite scaffold and its inherent mechanical properties.

Mechanical properties are important for an ideal skin substitute.[31,50] While the scaffold should be elastic, it should be strong enough to withstand regular forces that native skin normally undergoes and possess enough elongation before rupturing under stress. Although adding PU to gelatin did not change the fiber size and interfiber distance of the scaffold, both the tensile strength and elongation were significantly increased. It should be noted that skin has a multicomponent and complicated structure, with a wide range of reported mechanical properties (UTS ranging from 500 kPa to 35 MPa;[52,53] modulus ranging from 1 kP to 100 MPa[50,53]). This wide range is dependent on the location of the skin in the body as well as sample preparation and the orientation of the applying force.[53] Hence, synthetic scaffolds may not always possess the necessary properties and behavior of the native skin. Therefore, one of the first objectives of generating tissue-engineering constructs for skin substitutes would be for it to have biomechanical properties that enable an optimal environmental niche for developing a new skin and not to necessarily have the same mechanical properties of the mature native skin. The results of the mechanical studies shown in Figure 1g reveal that although adding PU increases the initial stiffness of electrospun gelatin scaffolds, the elastic properties were improved over those of a popular commercial DRM. Further, the gelatin–PU composite has the potential to recapitulate the skin characteristic as the biomaterial degrades. These features are important to enable better outcomes for the skin substitute in terms of increased flexibility of the treated skin, particularly when applied in a patient's joint area. Note also that the UTS value for gelatin improved significantly by incorporating the PU, which shows that the new constructs can withstand larger forces. The combination of both increased UTS and modulus resulted in the PU contributing to greater elongation when compared with the two biologically

derived matrices, that is, gelatin and DRM. Hence, the composite material shows a greater ability to absorb energy before rupturing. Therefore, overall, Gel80–PU20 showed improved mechanical properties when compared to pure gelatin and even in some aspects of the commercial DRM.

A collagenase degradation assay was performed as an in vitro model to study the composite's propensity to undergo biodegradation. Whereas this assay does not replicate in vivo conditions, which will be highly variable depending on the degree of inflammation present at the time of implantation and during the wound healing period, it does give us a relative measure of degradation in comparison to established materials. The data must be interpreted with knowledge that collagenase is only one of the parameters that is involved in the in vivo process of scaffold degradation, but yet it is an important one. In the physiological environment, biodegradation processes will be modulated by the actual enzyme concentration, local inhibitors, and rate of neo-tissue generation during wound healing and, as a result, may be anticipated to proceed kinetically at very different rates than those shown in the current in vitro assay. However, such an in vitro assay can provide an estimation of how different materials and fabrication methods may affect the relative degradation of scaffolds. As anticipated, pure gelatin demonstrated the fastest, undergoing breakdown within a few hours. Polycarbonate urethane has been shown to undergo hydrolytic biodegradation in the presence of inflammatory enzymes such as cholesterol esterase.[54] Its introduction into the gelatin nanofibers here showed that at 20% PU, we were able to significantly delay the degradation of the gelatin scaffold while the gelatin scaffold's mechanical integrity was significantly enhanced.

FTIR spectra of the scaffolds after degradation assay (Figure 1j) show that on day 14, the typical gelatin peak in the region of 1630 cm^{-1} has been substantially reduced, whereas the characteristic PU peak in the 1200–1280 cm^{-1} region is still present. This shows that degradation is not uniform, and gelatin (that makes up 80% of the scaffold) degrades faster. The data also suggest that the PU is mainly responsible for the prolonged integrity of the scaffold. However, looking at the day 7 spectrum for Gel80–PU20 reveals that the typical gelatin peak near 1630 cm^{-1} is still present, confirming that when compared with the 3 h degradation rate of Gel100, when gelatin is blended with PU, its degradation rate decreases. This observation is believed to be in part associated with strong secondary interactions via hydrogen bonding, as both these polymers are capable of forming H-bonding.[55,56] It is reported that the degree of H-bonding significantly influences the degradation of such polymers.[48,54,57,58] This is a very important compensation because fast degrading scaffolds lack the ability to perform as effective skin substitutes in vivo, limiting the provisional environment for cell infiltration and proliferation as well as presenting a challenge for the accumulation of new ECM formation. The loss of Gel100's original structure in comparison with Gel80–PU20 for 7 days in the culture media is shown in Figure 1k, which confirmed the result of the collagenase degradation experiment. When comparing the current Gel80–PU20 construct versus DRM, the latter degraded substantially more slowly in the presence of collagenase solution, retaining its original shape and form (Figure S3). This prolonged resistance to scaffold remodeling is reported to be due to the collagenase-resistant design of the DRM scaffold attained by the presence of chondroitin sulfate and the material's

cross-linking process.[59] Gradual in vivo characterization is necessary in order to enable appropriate scaffold remodeling, which has a beneficial outcome for skin reconstitution.[7]

It was observed that the HDFs were highly aligned on Gel100 (Figure 2a) and showed a high level of α-SMA, indicating that the fibroblasts were being differentiated toward a more contractile state[31] than cells within the G80–PU20 and DRM control. It has been reported that a rapid loss of tensile strength and/or fast degradation of the scaffold can lead to a contractile state, the characteristic of myofibroblasts found during granulation tissue formation.[60] Further, such a condition is reported to lead to more scarring in vivo.[31]

An ideal scaffold should allow cells to infiltrate and proliferate in order to fully cellularize the scaffold.[14] In the current study, it was shown that cells had more of a spindlelike morphology for the electrospun scaffolds, whereas a more polygonal morphology was visible on DRM (Figure 2b). For the latter, the polygonal morphology resulted from cell growth on the walls of the large pores within DRM. However, cells on the electrospun scaffolds were able to move between different fibers and were provided with a 3D fiber matrix that was more similar to that of the natural ECM structure.[9]

Typically, faster and greater cell infiltration is accompanied by a more rapid formation of granulation tissue, which in turn will accelerate the wound-healing process.[61] Intrinsically, the smaller initial pore dimensions in the electrospun scaffolds in comparison to freeze-dried scaffolds like DRM may have been anticipated to be a challenge for cell infiltration in this application; however, this was not observed. Considering the thickness of the scaffolds (~750 μm), cells infiltrate to a depth of about 60–80 μm after 7 days, equal to about 10% of the thickness. The observation of minimal differences between the Gel80–PU20 and DRM scaffolds shows that the presence of the larger pores in the scaffold (as seen in DRM) was not sufficient to accelerate cell infiltration in vitro and that other strategies, such as using stem cells to stimulate cell migration or promoting vascular network formation,[62–64] may be needed to further enhance cell migration.

Masson’s trichrome staining was performed to visualize the structure of the wound as well as the new tissue formed during the 20 days of scaffold transplantation in mice wounds (Figure 3a,b). It is seen that the cells have infiltrated into both the scaffolds from the wound bed. Although there was more cellularity at zone 1 within Figure 3a (bottom part close to the wound bed) showing the newly formed dermis, more scaffold could be visualized on the upper part (zone 3). This confirmed that the cells infiltrated into the scaffold, likely from the wound bed, and migrated to the upper level of the scaffold. As they infiltrated, they degraded the scaffold, highlighting the degradability of the Gel80–PU20 scaffold (further confirming the in vitro findings in Figure 1i) and enabled cell infiltration at least to the amount that is seen in DRM. In vivo scaffold degradation was quantified using H&E staining images (Figure 3f), and in accordance with our in vitro findings, we observed significantly more degradation in the Gel80–PU20 scaffold when compared with DRM over 20 days on the mouse wound.

Staining the tissue sections for the CD31 marker (Figure 3c,d) revealed blood vessels in the wound area and the scaffolds. Quantification of blood vessel population showed no

significant difference between Gel80–PU20 and DRM. This supports the capacity of the electrospun scaffold for integration to the wound bed and provides nutrients and oxygen to the newly formed tissue. Surface area measurements revealed that more surface area is covered by blood vessels in DRM in comparison with Gel80–PU20. This may be due to the larger pore dimensions for the DRM in comparison to the observed smaller interfiber distances in Gel80–PU20.

F4/80 immunostaining was performed to differentiate the cellular characteristics of infiltrated cells, distinguishing macrophages from fibroblasts in the wound area and in the scaffold region. This also provided an opportunity to verify the extent of inflammation (Figure 4a). The results showed that few macrophages were found on the electrospun scaffold, whereas the macrophage presence can be seen to be more prominent in several areas of the wound bed with DRM (S10). Also, when compared with DRM, a lower percentage of $F4/80^+$ macrophages was observed on the Gel80–PU20 scaffold. The relatively lower level of staining for macrophages may indicate that the scaffold does not elicit (or at least shows a milder) foreign body response or chronic inflammation after transplantation[61,65,66] and enables the granulation tissue to mature, shifting to the remodeling phase and hence with the potential to lead to less fibrosis and contractile tissue. MHC-II and CD206 markers have been used previously to stain M1 and M2 macrophages.[67] Similar to the F4/80 staining results, our data revealed that fewer macrophages (from either types) were present on the electrospun scaffold when compared with DRM (Figure 4b). Looking at the population of the two major types of macrophages showed that both types of macrophages were present on the scaffold, presumably indicating remodeling and a shift from the inflammatory to regeneration state.

α-SMA staining depicted in Figure 4c exposes stress fibers in the myofibroblasts as a sign of contraction in the wound bed. Myofibroblasts form after the migration of fibroblasts to the wound site in response to the cytokines released by inflammatory cells.[68] The ECM's mechanical microenvironment can also promote the differentiation of fibroblasts to myofibroblasts.[68] In normal wound repair, fibroblasts will align parallel to the wound bed in order to stretch and close the edges of the wound.[69] Normally, a prolonged presence of myofibroblasts leads to wound contraction and fibrosis and sometimes hypertrophic scarring.[70,71] It was observed that the presence of a cell-adherent scaffold with randomly oriented features can lead to a random orientation of the contractile cells, minimizing the overall macroscopic force vector and also attenuating contraction.[69] Hence, preventing myofibroblast formation is considered as being a good strategy to decrease tissue contraction.[68]

The images in Figure S12 provide a close look at the favorable outcome of the Gel80–PU20 scaffold when compared to a nonscaffold condition. It was observed that in the absence of any scaffold, a thick layer of cells stained with α-SMA elongated parallel to the wound could be seen, which shows that the wound is under contraction. However, when the wound is covered by the Gel80–PU20 scaffold, substantially fewer myofibroblasts could be seen, and the cells were not aligned parallel to the wound bed, characteristics of a less contractile state. This may in part be due to the randomly oriented fibers of the Gel80–PU20 scaffold.

Looking more closely at the α-SMA immunostaining data which showed that significantly more αSMA$^+$-myofibroblasts are present on the DRM when compared to Gel80–PU20 (Figure 3e), we can begin to take into consideration the difference in the modulus values seen in the mechanical studies, when DRM was compared to G80–PU20. These findings would suggest that G80–PU20 would be beneficial for decreasing wound contraction and scarring in favor of skin regeneration.

4. CONCLUSIONS

It was shown that the presence of PU enhanced the biostability of gelatin scaffolds and significantly improved the mechanical properties of the scaffold with no effect on the fiber size and morphology of the scaffold. The generation of these composites yielded good HDF viability for cell cultures on the scaffolds and led to a low myofibroblastic phenotype, both in vitro and in vivo. Cells were randomly oriented on Gel80–PU20, showing lower number of myofibroblasts (less α-SMA expression) unlike the cells on Gel100 which acquired an aligned orientation and yielded higher number of myofibroblasts. In spite of much smaller initial interfiber distances prior to HDF seeding for the as-made Gel80–PU20, when compared with DRM, the extent of cell infiltration was similar in both scaffolds. In vivo, the wound environment degraded the Gel80–PU20 scaffolds, and the cells penetrated deeply into the construct when the scaffold was placed on the mice wounds. Such scaffolds did not elicit a hyper-immune response and showed a significantly lower number of macrophages, accompanied by a lower number of myofibroblasts after 20 days, when compared with DRM. Overall the results show that the formation of the initial formulations of the Gel80–PU20 composite membrane provided a promising potential for an acellular skin substitute and a niche environment for HDFs, which may provide a future foundation for improved skin regeneration scaffolds when used with appropriate skin progenitor cells.[1]

5. EXPERIMENTAL SECTION

5.1. Materials.

Polycarbonate PU (~150 kDa) was synthesized using a previously established protocol.[35] Gelatin type A from pork skin (minimum bloom 225) was purchased from BioShop Canada. 1,1,1,3,3,3-Hexafluoro-2-propanol (HFIP) was obtained from Sigma-Aldrich. 1-Ethyl-3-(3-dimethylaminopropyl)carbodiimide hydrochloride (EDC) was purchased from Sigma. PBS, DMEM, fetal bovine serum (FBS), trypsin, and antibiotics were all obtained from MultiCell. HDFs were isolated from the intact human skin based on a previously described method.[72] A Live/Dead Viability Kit and an ActinGreen 488 ready probe were received from Life Technologies, NY. DAPI in mounting media was purchased from Sigma.

5.2. Methods.

5.2.1. Electrospinning.—A mixture of gelatin and PU (Gel80–PU20) with a final concentration of 13% w/v in HFIP was dissolved overnight on a vortex mixer and then fed into a 10 mL syringe. The distance between the syringe tip and the collecting surface (5 × 5 cm^2 aluminum foil) was 17 cm, and the voltage difference between them was set to 17 kV. Three milliliters of the solution was spun with a feed rate of 2 mL/h in order to

generate the gelatin and Gel80–PU20 scaffolds. This yielded a scaffold thickness of ~700 μm. Because of the high solubility of gelatin in aqueous media, these electrospun scaffolds were cross-linked by immersing in 50 mM EDC solution in ethanol overnight. Then, the scaffolds were washed in Milli-Q water three times, each for 1 h at room temperature.

5.2.2. Morphological and Chemical Characterization.—The morphology of the electrospun membranes was investigated using SEM and laser confocal microscopy. For SEM imaging, scaffolds were gold-sputtered with a Denton Desk II system to reach 20 nm gold thickness. Imaging was performed using a FEI XL30 ESEM microscope at a voltage of 20 kV and a working distance of 12 mm. The estimated average fiber diameter was determined from the SEM images by measuring the diameters of at least 200 fibers per test group using ImageJ. The estimated average interfiber distance was calculated by measuring the distance between the vertices and opposing sides of each polygon space made by fibers in the outermost sheet of the scaffold. At least 100 interfiber distances were measured for each test group. For imaging scaffolds after hydration, confocal microscopy was employed, taking advantage of the autofluorescence associated with the fibers at high intensity and prolonged exposure.

The chemical structure of the Gel–PU electrospun membranes was characterized by ATR–FTIR spectroscopy (Thermo Scientific iS50, USA). The transmittance of each membrane was recorded after 10 scans at a resolution of 4 cm^{-1} between 4000 and 550 cm^{-1}.

5.2.3. Microtensile Measurement.—The mechanical properties of the scaffolds were investigated via uniaxial microtensile testing on a tensile tester (Test Resources, model: 840L). Fully hydrated samples were cut to 0.5 mm × 4 mm rectangles and fixed between the two opposing clamps of the machine at a 20 mm distance. Tensile testing to failure was performed at a strain rate of 2 mm/min (10% strain/min) and using a force of 1 kg.

5.2.4. Swelling Index.—The swelling index of the scaffolds was calculated as the change in mass before and after hydration at room temperature. Scaffold samples were punched using an 8 mm punch and then freeze dried overnight, after which their mass was recorded as the dry mass. After recording the dry mass, the samples were soaked in DMEM media (Multicell) for 5 days. The scaffolds were then removed from DMEM, blot-dried, and weighed to measure the swollen mass. The swelling index is reported as the ratio of mass change before and after incubation in media to the initial weight.

5.2.5. Collagenase Degradation.—To characterize the rate of scaffold degradation, an in vitro collagenase degradation assay was undertaken. This assay was devised to mimic the enzymatic reactions that the scaffolds may experience in vivo. However, to shorten the length of the study and achieve a measurable difference between the scaffolds, a high concentration of collagenase (approximately 6 times that of the maximum concentration which typically forms during wound healing[73]) was used. Scaffolds of 8mm diameter were punched out of the electrospun membranes and were freeze-dried, weighed, and placed in 2 mL centrifuge tubes. Then, collagenase type I (Worthington Biochem. Corp., cat no. LS004197, ACT: 345 μ/mgdw) was dissolved in PBS at a concentration of 20 U/mL (58 μg/mL). Collagenase solution (500 μL) was added to each tube and placed in a humidified

oven at 37 °C for 1 h, 3 h, 6 h, 12 h, 1 day, 2 days, 3 days, 5 days, and 7 days. At each time point, the scaffolds were washed using deionized (DI) water, freeze-dried, and weighed again.

5.2.6. Cell Culture.—HDF were aseptically cultured in DMEM supplemented with 10% FBS and 1% penicillin/streptomycin at 37 °C and 5% CO_2 incubator. Media was changed two to three times a week under aseptic techniques, and the cells were passaged at 80% confluency. Hydrated scaffolds were soaked in PBS overnight and then left in separate wells in a two-well plate containing culture media for an hour before seeding the cells. The medium inside the wells was aspirated, and the cells were seeded on top of 6 mm round samples of the scaffolds (punched out of the electrospun membranes). The cells were used at passage 5–7 and seeded at a 3.5×10^4 cell–scaffold density before the addition of 1 mL of DMEM medium to each well. To enhance the seeding efficiency, the cells were added in a very small volume of media (i.e., 10 μL), and then 1 mL of culturing media was added after 15 min to enable sufficient adherence of the cells to the scaffold.

5.2.7. Cell Viability.—A Live/Dead Viability Kit was used for viability testing. After 7 days of culture, cell-seeded scaffolds were washed with PBS three times and then the viability reagent, including 0.5 μL/mL calcein AM and 2 μL/mL ethidium homodimer-1 (EthD) in 500 μL of Dulbecco's PBS, was added to the scaffolds and left in a 37 °C incubator for 45 min. Samples were then transferred to a chambered coverglass (Nunc Lab-Tek) and imaged immediately using a Zeiss Observer Z1 spinning disc confocal microscope (Zeiss). Live and dead cells were counted using ImageJ software (NIH).

5.2.8. Cell Adhesion and Morphological Staining.—To further investigate the cell–scaffold interaction, the cells were stained with ActinGreen (Alexa Fluor 488) and DAPI to stain F-actin and cell nuclei, respectively. Briefly, the scaffolds were washed with PBS three times and then fixed for 30 min using 4% paraformaldehyde in PBS. After 3× wash in ice-cold PBS, the scaffolds were permeabilized for 20 min with 0.5% Triton X-100 in PBS. Following 3× washing in PBS, ActinGreen was added dropwise (one droplet per 500 μL) to scaffold samples submerged in PBS and incubated for 30 min. Then, the samples were subjected to 3× washing with PBS. Following actin staining, one droplet of DAPI in mounting media was placed on each scaffold, and the samples were taken for imaging. Imaging was performed using a Zeiss Observer Z1 spinning disc confocal microscope (Zeiss).

5.2.9. α-SMA Expression.—To investigate α-SMA expression in the cells, anti-αSMA from eBioscience (14–9760-82) was used as a primary antibody, and donkey anti-mouse IgG (H + L) antibody (A-201202) from Thermo Fisher was used as the secondary antibody. After permeabilizing as in Section 5.2.8, the scaffold samples were washed 3× in PBS and blocked in 1% bovine serum albumin (BSA) in PBST (0.5% Triton X-100 in PBS) for 30 min. Then, the primary antibody was added to the scaffolds in PBST with a 1:500 dilution factor. The samples were placed overnight in a humidified chamber at 4 °C. The primary antibody was removed, and the scaffold went through 3× PBS washes. Then, the secondary antibody (diluted 1:500 in PBST) was added and left for 1 h at room temperature. After 3× PBS

washes, DAPI was added. Then, the scaffolds were transferred to a chambered coverglass for confocal imaging.

5.2.10. Animal Surgery Procedure.—All procedures were done as reported in a previous publication[72] and complied with the guidelines of the Sunnybrook Research Institute, Sunnybrook Health Sciences Centre Policy and Welfare Committee of the University of Toronto (Protocol# 14–503). Ten male WT BL6 mice (8 weeks, Jackson Laboratory) were anesthetized by inhalation of isoflurane in oxygen; then the dorsum was shaved. Two full-thickness excisional wounds were created using 8 mm punch biopsies on the upper back of the mice on either side from the midline (previously described[72]). To prevent skin contraction, a plastic 8 mm dome insert (described previously[51]) was placed in the wound, and then the scaffold was placed inside the domes with complete contact with the wound. The dome cap was closed, and the mice were placed in new cages with isopads. The mice and domes were checked once a day for 20 days. The mice were euthanized by CO_2 inhalation, and the wounds were excised along with 2 mm of satellite skin. The collected tissues were placed in formalin overnight and then sent for histology in 100% ethanol. The samples were embedded in paraffin, sectioned to 5 μm-thick slices using a microtome, and fixed on coverslips for future staining. Only wounds that continued to have their dome intact until the end of the experiment were used for analysis. The opaque dome prevented macroscopic observation during the implant period.

5.2.11. Masson's Trichrome Staining.—Trichrome reagents were obtained from Electron Microscopy Sciences, unless otherwise stated. After heating the paraffin-embedded slides of excised wounds at 60 °C, the slides were deparaffinized with citrosol twice (2 × 3 min) and rehydrated through 100% ethanol (×2), 95% ethanol, and 70% ethanol (3 min each) followed by washing in distilled water. Then, the slides were refixed in Bouin's solution overnight at room temperature. After 10 min of rinsing in running tap water, the tissues were stained in Weigert's iron hematoxylin working solution (Sigma-Aldrich) for 10 min, rinsed in running warm tap water for 10 min, and briefly washed in distilled water. The slides were stained in Biebrich scarlet-acid fuchsin solution for 15 min, washed in distilled water, and differentiated in phosphomolybdic–phosphotungstic acid solution for 15 min. The slides were then transferred directly to aniline blue solution and stained for 10 min, followed by a brief rinse in distilled water. In the next step, the sections were differentiated in 1% acetic acid solution for 5 min, washed in distilled water, and dehydrated very quickly through 95% ethanol and 100% ethanol (30 s each) and then cleared in citrosol (1 min). Finally, the sections were mounted with a xylene-based mounting medium (Triangle Biomedical Sciences).

5.2.12. IHC and IF.—Following deparaffinization and rehydration, 1× antigen decloaker solution (Biocare Medical) was placed in the decloaking chamber and preheated at 70 °C for 20 min. Next, the slides were placed in the slide jar, and the chamber was set to heat the solution and slides at 110 °C for 4 min and then cooled to 50 °C. The slides were washed under running water followed by distilled water before the blocking step. A hydrophobic pen was used to draw a circle around every wound on the slides. Wounds were blocked with 3% H_2O_2 for 10 min and washed with washing buffer (0.05 M Tris–HCl, 0.15 M NaCl, and

0.05% Tween 20 in DI water). The sections were incubated with a primary antibody in PBS for 1 h at room temperature. Anti-αSMA antibody (1:100; eBioscience) and F4/80 antibody (1:200; AbD Serotec) were used as the primary antibodies.

The slides were then washed with washing buffer and incubated in the MACH3 probe (Biocare Medical) that matches the primary antibody species for 15 min. Following another buffer wash, the slides were incubated for 15 min in the MACH3 horseradish peroxidase polymer to enable detection corresponding to the species-specific probe in the last step. After another buffer wash, the sections were incubated with betazoid diaminobenzidine chromogen kits (Biocare Medical) for up to 10 min until a visible brown color occurred. Following rinsing with running tap water, the slides were counter-stained with hematoxylin for 30 s and underwent another rinse with tap water. The slides were then differentiated in 1.5% acid alcohol for three dips, rinsed with tap water, and stained in 0.1% sodium bicarbonate for 10 s. After this, the slides were dehydrated in 95 and 100% ethanol and citrosol solutions and mounted on a coverslip using the xylene-based mounting medium.

For IF staining of the slides, deparaffinization and antigen retrieval using antigen decloaker were carried out as described above. After the washing process, the sections were permeablized in PBST (PBS containing 0.25% Triton X-100) for 10 min, washed in PBS three times for 5 min, and incubated with 1% BSA in PBST for 30 min (to block nonspecific binding of the antibodies). Then, they were incubated in the primary antibody dissolved in 1% BSA in PBST in a humidified chamber for 1 h at room temperature. The mixture solution was decanted, and the slides were washed three times in PBS and incubated with a secondary antibody (which were raised in different species) dissolved in 1% BSA solution for 1 h at room temperature in the dark. Then, the secondary antibody solution was decanted, and the slides were washed three times with PBS. If biotinylated, staining was followed by 20 min room-temperature incubation with streptavidin (1:5000) and washed three times. The coverslips were mounted with a drop of mounting medium containing DAPI, sealed with a nail polish to prevent drying and movement under the microscope, and stored in the dark at 4 °C.

5.3. Statistics.

All data are shown as a mean ± experimental standard deviation. Student's t-test and one-way analysis of variance test were used to determine the statistical significance as indicated in the figures by an * ($P < 0.05$). All experiments were repeated three times, in which at least three samples were measured for each condition in each experiment.

Supplementary Material

Refer to Web version on PubMed Central for supplementary material.

ACKNOWLEDGMENTS

The authors appreciate funding from the following sources to carry out this research: Toronto Hydro, the Canadian Institutes of Health research no. 123336, CFI Leader's Opportunity Fund: project no. 25407, Medicine by Design Seed award, and NIH RO1 GM087285-01.

REFERENCES

(1). Amini-Nik S; Dolp R; Eylert G; Datu A; Parousis A; Blakeley C; Jeschke MG Stem cells derived from burned skin—The future of burn care. EBioMedicine 2018, 37, 509–520. [PubMed: 30409728]

(2). Sun BK; Siprashvili Z; Khavari PA Advances in skin grafting and treatment of cutaneous wounds. Science 2014, 346, 941–945. [PubMed: 25414301]

(3). MacNeil S Progress and opportunities for tissue-engineered skin. Nature 2007, 445, 874–880. [PubMed: 17314974]

(4). Jeschke MG; Patsouris D; Stanojcic M; Abdullahi A; Rehou S; Pinto R; Chen P; Burnett M; Amini-Nik S Pathophysiologic Response to Burns in the Elderly. EBioMedicine 2015, 2, 1536–1548. [PubMed: 26629550]

(5). Jeschke MG; Pinto R; Costford SR; Amini-Nik S Threshold age and burn size associated with poor outcomes in the elderly after burn injury. Burns 2016, 42, 276–281. [PubMed: 26803373]

(6). Yannas IV; Lee E; Orgill DP; Skrabut EM; Murphy GF Synthesis and Characterization of a Model Extracellular Matrix That Induces Partial Regeneration of Adult Mammalian Skin. Proc. Natl. Acad. Sci. U.S.A 1989, 86, 933–937. [PubMed: 2915988]

(7). Shahrokhi S; Arno A; Jeschke MG The Use of Dermal Substitutes in Burn Surgery: Acute Phase. Wound Repair Regen 2014, 22, 14–22.

(8). Schulz JT III; Tompkins RG; Burke JF Artificial Skin. Annu. Rev. Med 2000, 51, 231–244. [PubMed: 10774462]

(9). Sheikholeslam M; Wright MEE; Jeschke MG; Amini-Nik S Biomaterials for Skin Substitutes. Adv. Healthcare Mater 2018, 7, 1700897.

(10). Chua AWC; Khoo YC; Tan BK; Tan KC; Foo CL; Chong SJ Skin Tissue Engineering Advances in Severe Burns: Review and Therapeutic Applications. Burn. Trauma 2016, 4, 3.

(11). Wang Y; Beekman J; Hew J; Jackson S; Issler-Fisher AC; Parungao R; Lajevardi SS; Li Z; Maitz PKM Burn Injury: Challenges and Advances in Burn Wound Healing, Infection, Pain and Scarring. Adv. Drug Delivery Rev 2018, 123, 3–17.

(12). Wong VW; Levi B; Rajadas J; Longaker MT; Gurtner GC Stem cell niches for skin regeneration. Int J Biomater 2012, 2012, 926059. [PubMed: 22701121]

(13). Bielefeld KA; Amini-Nik S; Alman BA Cutaneous Wound Healing: Recruiting Developmental Pathways for Regeneration. Cell. Mol. Life Sci 2013, 70, 2059–2081. [PubMed: 23052205]

(14). Nicholas MN; Jeschke MG; Amini-Nik S Methodologies in creating skin substitutes. Cell. Mol. Life Sci 2016, 73, 3453–3472. [PubMed: 27154041]

(15). Atala A; Kasper FK; Mikos AG Engineering Complex Tissues. Sci. Transl. Med 2012, 4, 1–11.

(16). Groeber F; Holeiter M; Hampel M; Hinderer S; Schenke-Layland K Skin Tissue Engineering—In Vivo and in Vitro Applications. Adv. Drug Delivery Rev 2011, 63, 352–366.

(17). Zhong SP; Zhang YZ; Lim CT Tissue Scaffolds for Skin Wound Healing and Dermal Reconstruction. Wiley Interdiscip. Rev.: Nanomed. Nanobiotechnol 2010, 2, 510–525. [PubMed: 20607703]

(18). Hu MS; Maan ZN; Wu J-C; Rennert RC; Hong WX; Lai TS; Cheung ATM; Walmsley GG; Chung MT; McArdle A; Longaker MT; Lorenz HP Tissue Engineering and Regenerative Repair in Wound Healing. Ann. Biomed. Eng 2014, 42, 1494–1507. [PubMed: 24788648]

(19). Norouzi M; Boroujeni SM; Omidvarkordshouli N; Soleimani M Advances in Skin Regeneration: Application of Electrospun Scaffolds. Adv. Healthcare Mater 2015, 4, 1114–1133.

(20). Agarwal S; Wendorff JH; Greiner A Use of Electrospinning Technique for Biomedical Applications. Polymer 2008, 49, 5603–5621.

(21). Bhardwaj N; Kundu SC Electrospinning: A Fascinating Fiber Fabrication Technique. Biotechnol. Adv 2010, 28, 325–347. [PubMed: 20100560]

(22). Pham QP; Sharma U; Mikos AG Electrospinning of Polymeric Nanofibers for Tissue Engineering Applications: A Review. Tissue Eng 2006, 12, 1197–1211. [PubMed: 16771634]

(23). Norouzi M; Boroujeni SM; Omidvarkordshouli N; Soleimani M Advances in Skin Regeneration: Application of Electrospun Scaffolds. Adv. Healthcare Mater 2015, 4, 1114–1133.

(24). Rho KS; Jeong L; Lee G; Seo B; Park YJ; Hong S; Roh S; Cho JJ; Park WH; Min B Electrospinning of Collagen Nanofibers: Effects on the Behavior of Normal Human Keratinocytes and Early-Stage Wound Healing. Biomaterials 2006, 27, 1452–1461. [PubMed: 16143390]

(25). Powell HM; Boyce ST Fiber Density of Electrospun Gelatin Scaffolds Regulates Morphogenesis of Dermal-Epidermal Skin Substitutes. J. Biomed. Mater. Res., Part A 2008, 84, 1078–1086.

(26). Nivison-Smith L; Rnjak J; Weiss AS Synthetic Human Elastin Microfibers: Stable Cross-Linked Tropoelastin and Cell Interactive Constructs for Tissue Engineering Applications. Acta Biomater 2010, 6, 354–359. [PubMed: 19671457]

(27). Sajkiewicz P; Kołbuk D Electrospinning of Gelatin for Tissue Engineering—Molecular Conformation as One of the Overlooked Problems. J. Biomater. Sci., Polym. Ed 2014, 25, 2009–2022. [PubMed: 25357002]

(28). Kang H-W; Tabata Y; Ikada Y Fabrication of Porous Gelatin Scaffolds for Tissue Engineering. Biomaterials 1999, 20, 1339–1344. [PubMed: 10403052]

(29). Choi YS; Hong SR; Lee YM; Song KW; Park MH; Nam YS Study on Gelatin-Containing Artificial Skin: I. Preparation and Characteristics of Novel Gelatin-Alginate Sponge. Biomaterials 1999, 20, 409–417. [PubMed: 10204983]

(30). Rnjak J; Wise SG; Mithieux SM; Weiss AS Severe Burn Injuries and the Role of Elastin in the Design of Dermal Substitutes. Tissue Eng., Part B 2011, 17, 81–91.

(31). Lorden ER; Miller KJ; Bashirov L; Ibrahim MM; Hammett E; Jung Y; Medina MA; Rastegarpour A; Selim MA; Leong KW; Levinson H Mitigation of Hypertrophic Scar Contraction via an Elastomeric Biodegradable Scaffold. Biomaterials 2015, 43, 61–70. [PubMed: 25591962]

(32). McBane JE; Sharifpoor S; Cai K; Labow RS; Santerre JP Biodegradation and in Vivo Biocompatibility of a Degradable, Polar/Hydrophobic/Ionic Polyurethane for Tissue Engineering Applications. Biomaterials 2011, 32, 6034–6044. [PubMed: 21641638]

(33). Cheung JWC; McCulloch CAG; Santerre JP Establishing a Gingival Fibroblast Phenotype in a Perfused Degradable Polyurethane Scaffold: Mediation by TGF-β1, FGF-2, β1-Integrin, and Focal Adhesion Kinase. Biomaterials 2014, 35, 10025–10032. [PubMed: 25282621]

(34). Cheung JWC; Jain D; McCulloch C. a G.; Santerre JP. Pro-Angiogenic Character of Endothelial Cells and Gingival Fibroblasts Cocultures in Perfused Degradable Polyurethane Scaffolds. Tissue Eng., Part A 2015, 21, 1–13. [PubMed: 25425342]

(35). Yang L; Kandel RA; Chang G; Santerre JP Polar Surface Chemistry of Nanofibrous Polyurethane Scaffold Affects Annulus Fibrosus Cell Attachment and Early Matrix Accumulation. J. Biomed. Mater. Res., Part A 2009, 91, 1089–1099.

(36). Yeganegi M; Kandel RA; Santerre JP Characterization of a Biodegradable Electrospun Polyurethane Nanofiber Scaffold: Mechanical Properties and Cytotoxicity. Acta Biomater 2010, 6, 3847–3855. [PubMed: 20466079]

(37). Detta N; Errico C; Dinucci D; Puppi D; Clarke DA; Reilly GC; Chiellini F Novel Electrospun Polyurethane/Gelatin Composite Meshes for Vascular Grafts. J. Mater. Sci.: Mater. Med 2010, 21, 1761–1769. [PubMed: 20135202]

(38). Wang H; Feng Y; Behl M; Lendlein A; Zhao H; Xiao R; Lu J; Zhang L; Guo J Hemocompatible Polyurethane/Gelatin-Heparin Nanofibrous Scaffolds Formed by a Bi-Layer Electrospinning Technique as Potential Artificial Blood Vessels. Front. Chem. Eng. China 2011, 5, 392–400.

(39). Nagiah N; Johnson R; Anderson R; Elliott W; Tan W Highly Compliant Vascular Grafts with Gelatin-Sheathed Coaxially Structured Nanofibers. Langmuir 2015, 31, 12993–13002. [PubMed: 26529143]

(40). Wang N; Burugapalli K; Wijesuriya S; Far MY; Song W; Moussy F; Zheng Y; Ma Y; Wu Z; Li K Electrospun Polyurethane-Core and Gelatin-Shell Coaxial Fibre Coatings for Miniature Implantable Biosensors. Biofabrication 2014, 6, 015002. [PubMed: 24346001]

(41). Kim SE; Heo DN; Lee JB; Kim JR; Park SH; Jeon SH; Kwon IK Electrospun Gelatin/Polyurethane Blended Nanofibers for Wound Healing. Biomed. Mater 2009, 4, 044106. [PubMed: 19671952]

(42). Heo DN; Yang DH; Lee JB; Bae MS; Kim JH; Moon SH; Chun HJ; Kim CH; Lim HN; Kwon IK Burn-Wound Healing Effect of Gelatin/Polyurethane Nanofiber Scaffold Containing Silver-Sulfadiazine. J. Biomed. Nanotechnol 2013, 9, 511–515. [PubMed: 23621008]

(43). Sarkar S; Chourasia A; Maji S; Sadhukhan S; Kumar S; Adhikari B Synthesis and Characterization of Gelatin Based Polyester Urethane Scaffold. Bull. Mater. Sci 2006, 29, 475–484.

(44). Lee TJ; Kwon SH; Kim BK Biodegradable Sol–Gel Coatings of Waterborne Poly-Urethane/Gelatin Chemical Hybrids. Prog. Org. Coat 2014, 77, 1111–1116.

(45). Vatankhah E; Prabhakaran MP; Semnani D; Razavi S; Zamani M; Ramakrishna S Phenotypic Modulation of Smooth Muscle Cells by Chemical and Mechanical Cues of Electrospun Tecophilic/Gelatin Nanofibers. ACS Appl. Mater. Interfaces 2014, 6, 4089–4101. [PubMed: 24588215]

(46). Jamadi ES; Ghasemi-Mobarakeh L; Morshed M; Sadeghi M; Prabhakaran MP; Ramakrishna S Synthesis of Polyester Urethane Urea and Fabrication of Elastomeric Nanofibrous Scaffolds for Myocardial Regeneration. Mater. Sci. Eng., C 2016, 63, 106–116.

(47). Vieira T; Silva JC; Borges JP; Henriques C Synthesis, Electrospinning and in Vitro Test of a New Biodegradable Gelatin-Based Poly(Ester Urethane Urea) for Soft Tissue Engineering. Eur. Polym. J 2018, 103, 271–281.

(48). Tang YW; Labow RS; Santerre JP Enzyme Induced Biodegradation of Polycarbonate-Polyurethanes: Dose Dependence Effect of Cholesterol Esterase. Biomaterials 2003, 24, 2003–2011. [PubMed: 12628819]

(49). Pezeshki-Modaress M; Mirzadeh H; Zandi M Gelatin-GAG Electrospun Nanofibrous Scaffold for Skin Tissue Engineering: Fabrication and Modeling of Process Parameters. Mater. Sci. Eng., C 2015, 48, 704–712.

(50). Achterberg VF; Buscemi L; Diekmann H; Smith-Clerc J; Schwengler H; Meister JJ; Wenck H; Gallinat S; Hinz B The Nano-Scale Mechanical Properties of the Extracellular Matrix Regulate Dermal Fibroblast Function. J. Invest. Dermatol 2014, 134, 1862–1872. [PubMed: 24670384]

(51). Jeschke MG; Sadri A-R; Belo C; Amini-Nik S A Surgical Device to Study the Efficacy of Bioengineered Skin Substitutes in Mice Wound Healing Models. Tissue Eng., Part C 2017, 23, 237–242.

(52). Lorden ER; Miller KJ; Ibrahim MM; Bashirov L; Hammett E; Chakraborty S; Quiles-Torres C; Selim MA; Leong KW; Levinson H Biostable Electrospun Microfibrous Scaffolds Mitigate Hypertrophic Scar Contraction in an Immune-Competent Murine Model. Acta Biomater 2016, 32, 100–109. [PubMed: 26708709]

(53). Ní Annaidh A; Bruyère K; Destrade M; Gilchrist MD; Otténio M Characterization of the Anisotropic Mechanical Properties of Excised Human Skin. J. Mech. Behav. Biomed. Mater 2012, 5, 139–148. [PubMed: 22100088]

(54). Tang YW; Labow RS; Santerre JP Enzyme-Induced Biodegradation of Polycarbonate-Polyurethanes: Dependence on Hard-Segment Chemistry. J. Biomed. Mater. Res 2001, 57, 597–611. [PubMed: 11553891]

(55). Cheng M; Deng J; Yang F; Gong Y; Zhao N; Zhang X Study on Physical Properties and Nerve Cell Affinity of Composite Films from Chitosan and Gelatin Solutions. Biomaterials 2003, 24, 2871–2880. [PubMed: 12742725]

(56). Wright MEE; Wong AT; Levitt D; Parrag IC; Yang M; Santerre JP Influence of Ciprofloxacin-Based Additives on the Hydrolysis of Nanofiber Polyurethane Membranes. J. Biomed. Mater. Res., Part A 2018, 106, 1211–1222.

(57). Wright MEE; Wong AT; Levitt D; Parrag IC; Yang M; Santerre JP Influence of Ciprofloxacin-Based Additives on the Hydrolysis of Nanofiber Polyurethane Membranes. J. Biomed. Mater. Res., Part A 2018, 106, 1211–1222.

(58). Tang YW; Labow RS; Santerre JP Enzyme-induced Biodegradation of Polycarbonate Polyurethanes: Dependence on Hard-segment Concentration. J. Biomed. Mater. Res 2001, 56, 516–528. [PubMed: 11400129]

(59). Yannas IV; Burke JF Design of an artificial skin. I. Basic design principles. J. Biomed. Mater. Res.J. Biomed. Mater. Res 1980, 14, 65–81. [PubMed: 6987234]

(60). Amini-Nik S; Yousuf Y; Jeschke MG Scar Management in Burn Injuries Using Drug Delivery and Molecular Signaling: Current Treatments and Future Directions. Advanced Drug Delivery Reviews; Elsevier, July 27, 2018; pp 135–154. [PubMed: 28757325]

(61). Gurtner GC; Werner S; Barrandon Y; Longaker MT Wound repair and regeneration. Nature 2008, 453, 314–321. [PubMed: 18480812]

(62). Kim W-S; Park B-S; Sung J-H; Yang J-M; Park S-B; Kwak S-J; Park J-S Wound Healing Effect of Adipose-Derived Stem Cells: A Critical Role of Secretory Factors on Human Dermal Fibroblasts. J. Dermatol. Sci 2007, 48, 15–24. [PubMed: 17643966]

(63). Freiman A; Shandalov Y; Rozenfeld D; Shor E; Segal S; Ben-David D; Meretzki S; Egozi D; Levenberg S Adipose-Derived Endothelial and Mesenchymal Stem Cells Enhance Vascular Network Formation on Three-Dimensional Constructs in Vitro. Stem Cell Res. Ther 2016, 7, 5. [PubMed: 26753517]

(64). Bakhtyar N; Jeschke MG; Herer E; Sheikholeslam M; Amini-Nik S Exosomes from Acellular Wharton's Jelly of the Human Umbilical Cord Promotes Skin Wound Healing. Stem Cell Res. Ther 2018, 9, 1–14. [PubMed: 29291747]

(65). Sun G; Zhang X; Shen Y; Sebastian R; Dickinson LE; Fox-talbot K; Reinblatt M; Steenbergenc C; Harmonb JW; Gerecht S Dextran Hydrogel Scaffolds Enhance Angiogenic Responses and Promote Complete Skin Regeneration during Burn Wound Healing. Proc. Natl. Acad. Sci. U.S.A 2011, 108, 20976–20981. [PubMed: 22171002]

(66). Shen Y-I; Song H-HG; Papa AE; Burke JA; Volk SW; Gerecht S Acellular Hydrogels for Regenerative Burn Wound Healing: Translation from a Porcine Model. J. Invest. Dermatol 2015, 135, 2519–2529. [PubMed: 26358387]

(67). Biglari S; Le TYL; Tan RP; Wise SG; Zambon A; Codolo G; De Bernard M; Warkiani M; Schindeler A; Naficy S; Valtchev P; Khademhosseini A; Dehghani F Simulating Inflammation in a Wound Microenvironment Using a Dermal Wound-on-a-Chip Model. Adv. Healthcare Mater 2019, 8, 1801307.

(68). Hinz B; Phan SH; Thannickal VJ; Galli A; Bochaton-Piallat ML; Gabbiani G The Myofibroblast: One Function, Multiple Origins. Am. J. Pathol 2007, 170, 1807–1816. [PubMed: 17525249]

(69). Soller EC; Tzeranis DS; Miu K; So PTC; Yannas IV Common Features of Optimal Collagen Scaffolds That Disrupt Wound Contraction and Enhance Regeneration Both in Peripheral Nerves and in Skin. Biomaterials 2012, 33, 4783–4791. [PubMed: 22483241]

(70). Tomasek JJ; Gabbiani G; Hinz B; Chaponnier C; Brown RA Myofibroblasts and Mechano-Regulation of Connective Tissue Remodelling. Nat. Rev. Mol. Cell Biol 2002, 3, 349–363. [PubMed: 11988769]

(71). Li CX; Talele NP; Boo S; Koehler A; Knee-Walden E; Balestrini JL; Speight P; Kapus A; Hinz B MicroRNA-21 Preserves the Fibrotic Mechanical Memory of Mesenchymal Stem Cells. Nat. Mater 2017, 16, 379–389. [PubMed: 27798620]

(72). Nicholas MN; Jeschke MG; Amini-Nik S Cellularized Bilayer Pullulan-Gelatin Hydrogel for Skin Regeneration. Tissue Eng., Part A 2016, 229–10754764

(73). Ågren MS; Carolyn JT; Woessner JF; Eaglstein WH; Mertz PM Collagenase in Wound Healing: Effect of Wound Age and Type. J. Invest. Dermatol 1992, 99, 709–714. [PubMed: 1469286]

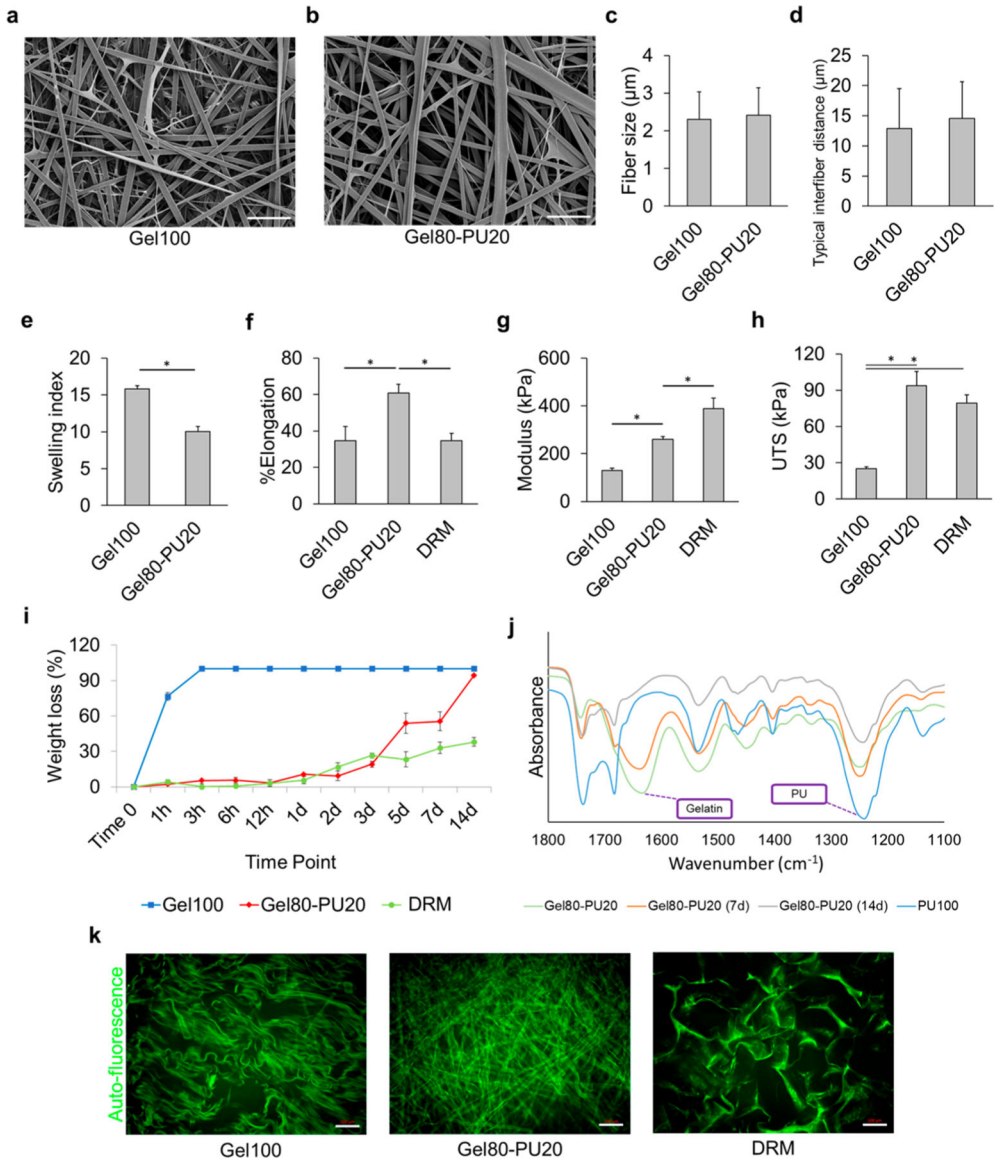

Figure 1.

SEM images of (a) Gel100 and (b) Gel80–PU20. The scale bar is 20 μm. (c,d) Average fiber size and typical interfiber distance of electrospun scaffolds, respectively. (e) Swelling index (ratio of mass change before and after incubation in media to the initial weight) for Gel100, Gel80–PU20, and DRM after incubating the scaffolds in DMEM media for 5 days. All groups are significantly different (Student's *t*-test, $*P < 0.05$). (f) Typical stress–strain curve for gelatin, Gel80–PU20, and DRM. (g) Elastic modulus and (h) UTS of the scaffolds. $*P < 0.05$. (i) Degradation of different scaffolds in 60 μg/mL collagenase in PBS at 37 °C after different time points. (j) FTIR spectra after collagenase degradation assay for Gel80–PU20 (note: PU100 reported here was intact and not degraded and only used as a relative control to identify PU chemical groups). Distinct peaks corresponding to pure PU and gelatin are labeled. (k) Acellular structure of each scaffold (kept in DMEM media for 7 days) revealed by autofluorescence. The scale bar is 100 μm.

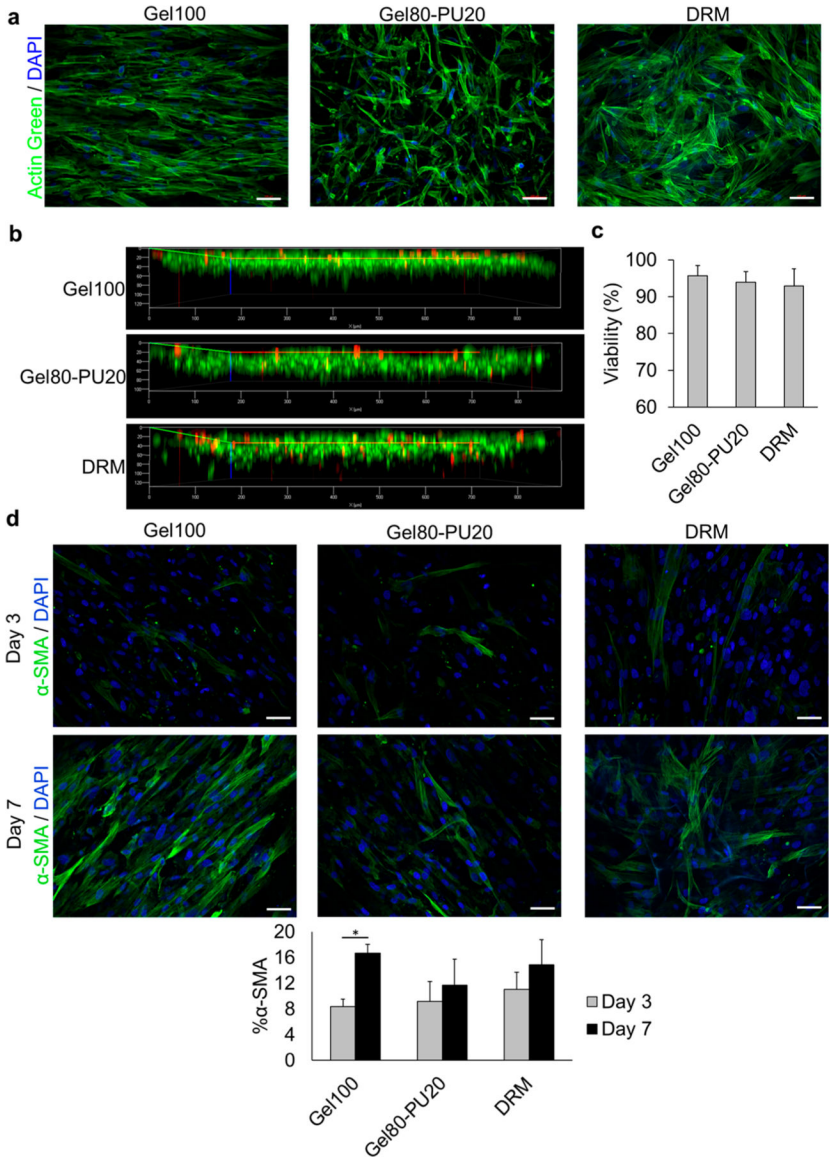

Figure 2.

(a) Cellular interaction with different scaffolds after 7 days: green = F-actin stained with ActinGreen (Alexa Fluor 488) and blue = DAPI in nuclei. (b) Cell penetration level into the scaffolds. (c) Cell viability measurement in each scaffold after Live/Dead staining and counting live and dead cells in the corresponding images. (d) α-SMA expression in HDF cells as a marker of myofibroblasts. Green = α-SMA positive cells and blue = DAPI in nucleus. Graph: quantification of α-SMA stress fiber-positive HDFs. The scale bar in all images is 100 μm.

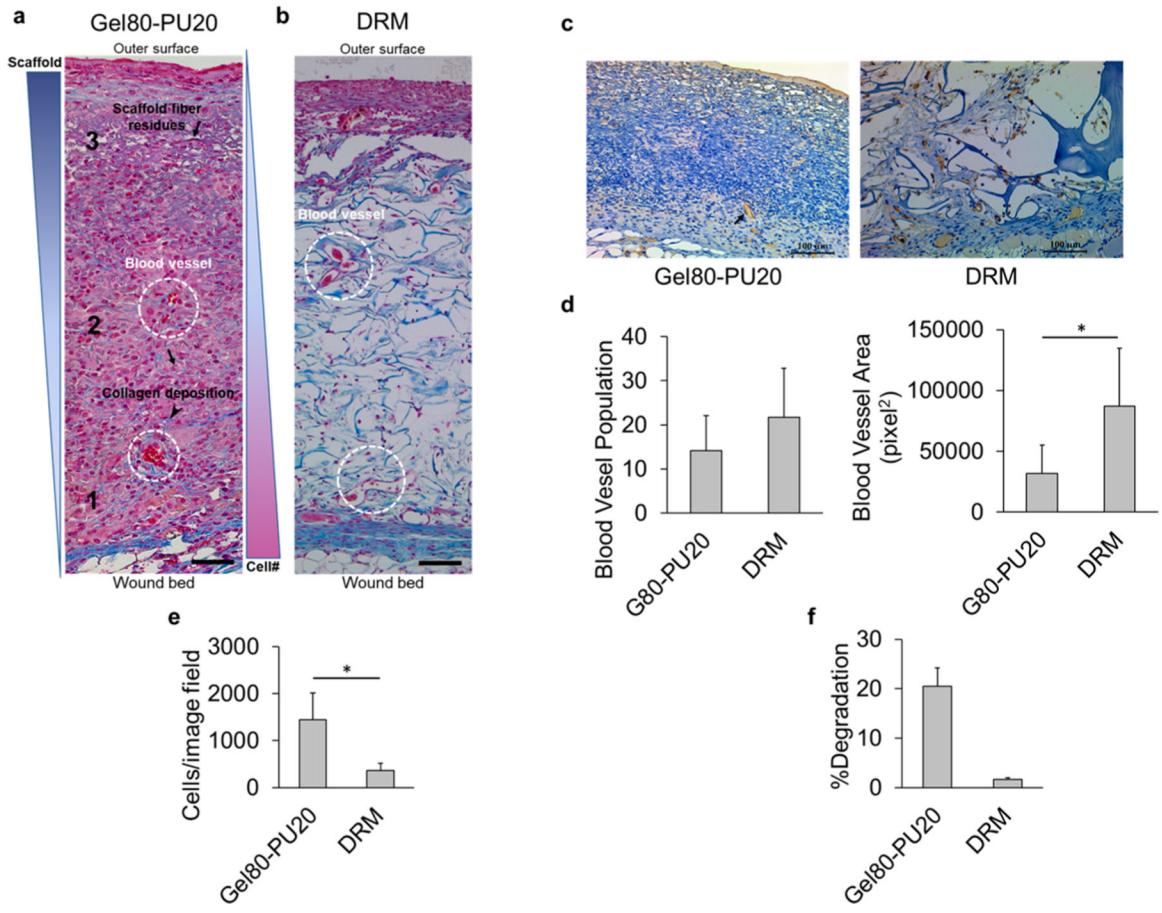

Figure 3.

(a) Trichrome staining of acellular electrospun Gel80–PU20 membranes on the mice after 20 days, illustrating cell infiltration from the wound bed (zone 1) to the surface (zone 3) at the center of the wound (arrows: scaffold fiber residues; arrow head: collagen deposition; dashed circles: blood vessels.). The scale bar is 50 μm. (b) Trichrome staining of acellular DRM after 20 days on the mice. The scale bar is 100 μm. (c) CD31 staining of acellular electrospun Gel80–PU20 membrane and DRM on the mice after 20 days, showing blood vessels. (d) Quantification of blood vessel population and area on the image field, $*P < 0.05$. (e) Scaffold cellularity quantification per image field shown in (a,b). (f) Scaffold degradation after 20 days on the wound.

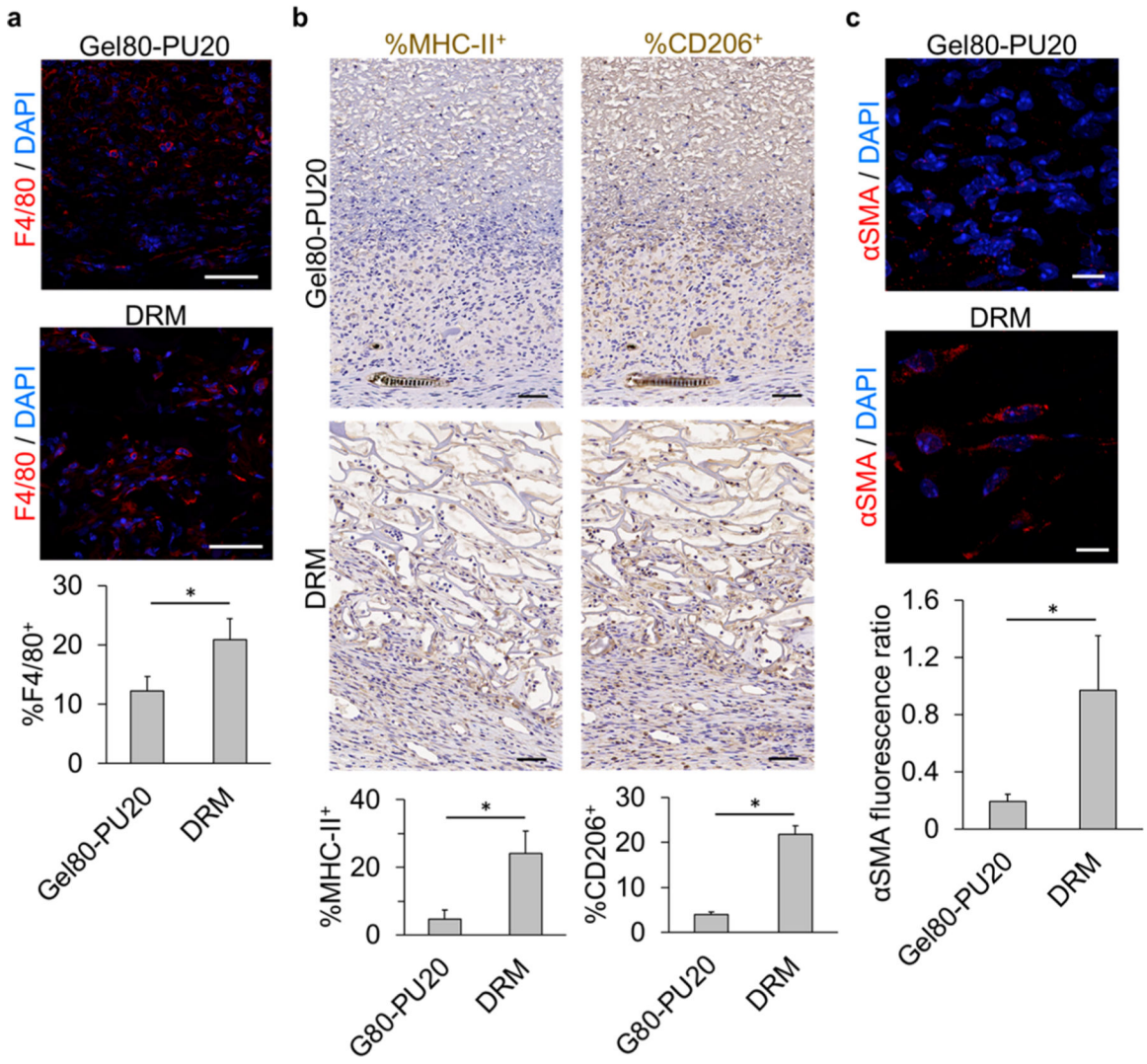

Figure 4.

Immunostaining of mouse wound sections covered by acellular electrospun Gel80–PU20 membrane and DRM after 20 days. (a) F4/80 staining for macrophages on the scaffolds and quantification of the F4/80$^+$ cells (*$P < 0.001$). The scale bar is 50 μm. (b) Staining for MHC-II (M1) and CD206 (M2) and quantification of the stained cells (*$P < 0.001$). The scale bar is 50 μm. (c) Assessing the scaffolds for the presence of αSMA$^+$ HDFs and quantification of the αSMA content by measuring the αSMA fluorescence ratio in each image field (*$P < 0.001$). The scale bar is 10 μm.

Table 1.

Description and Rationale for the Scaffolds Used in the Study

Gel100	positive control material to compare to gelatin–PU materials
Gel80–PU20	candidate scaffold showing a significant improvement over Gel100 without long degradation periods, which are typical of polycarbonate PUs[36]
DRM	an established commercial product that is being used clinically and is a collagen-based scaffold